Research Article | Vol. 6, No. 10 | 1 Oct 2016 | OPTICAL MATERIALS EXPRESS 3159

Optical Materials EXPRESS

Size-dependent saturable absorption and mode-locking of dispersed black phosphorus nanosheets

SAIFENG ZHANG,[1] XIAOYAN ZHANG,[1] HAO WANG,[2] BOHUA CHEN,[2] KAN WU,[2,5] KANGPENG WANG,[3,4] DAMIEN HANLON,[3,4] JONATHAN N. COLEMAN,[3,4] JIANPING CHEN,[2] LONG ZHANG,[1] AND JUN WANG[1,*]

[1]*Key Laboratory of Materials for High-Power Laser, Shanghai Institute of Optics and Fine Mechanics, Chinese Academy of Sciences, Shanghai 201800, China*
[2]*State Key Laboratory of Advanced Optical Communication Systems and Networks, Department of Electronic Engineering, Shanghai Jiao Tong University, Shanghai 200240, China*
[3]*School of Physics, Trinity College Dublin, Dublin 2, Ireland*
[4]*CRANN and AMBER Research Centres, Trinity College Dublin, Dublin 2, Ireland*
[5]*kanwu@sjtu.edu.cn*
[*]*jwang@siom.ac.cn*

Abstract: Size dependence of the saturable absorption (SA) property for black phosphorus (BP) was investigated. Three types of BP dispersions with different sizes were prepared using the liquid phase exfoliation method. By fitting the Z-scan data with the analytical solution of the propagation equation, the SA coefficients α_{NL} and the imaginary part of the third order optical susceptibility $\mathrm{Im}\,\chi^{(3)}$ are compared at two specific wavelengths, one above the bandgap of the BP monolayer at 515 nm and another between the bandgaps of the monolayer and bulk at 1030 nm. A figure of merit (FOM, $|\mathrm{Im}\chi^{(3)}/\alpha_0|$, α_0 linear absorption) was employed to assess the SA performance of the three different dispersions. The FOM, about $(2.1 \pm 0.3) \times 10^{-14}$ esu cm at 515 nm, hardly depends on the size and hence the layer number of the dispersed BP nanosheets, whereas that at 1030 nm decreases from $(1.14 \pm 0.20) \times 10^{-14}$ to $(0.50 \pm 0.02) \times 10^{-14}$ esu cm when the size of the nanosheets becomes smaller.

OCIS codes: (160.4330) Nonlinear optical materials; (140.3540) Lasers, Q-switched; (160.4236) Nanomaterials.

References and links

1. L. Li, Y. Yu, G. J. Ye, Q. Ge, X. Ou, H. Wu, D. Feng, X. H. Chen, and Y. Zhang, "Black phosphorus field-effect transistors," Nat. Nanotechnol. **9**(5), 372–377 (2014).
2. H. Liu, A. T. Neal, Z. Zhu, Z. Luo, X. Xu, D. Tománek, and P. D. Ye, "Phosphorene: an unexplored 2D semiconductor with a high hole mobility," ACS Nano **8**(4), 4033–4041 (2014).
3. A. Castellanos-Gomez, L. Vicarelli, E. Prada, J. O. Island, K. L. Narasimha-Acharya, S. I. Blanter, D. J. Groenendijk, M. Buscema, G. A. Steele, J. V. Alvarez, H. W. Zandbergen, J. J. Palacios, and H. S. J. van der Zant, "Isolation and characterization of few-layer black phosphorus," 2D Mater **1**(2), 025001 (2014).
4. S. B. Lu, L. L. Miao, Z. N. Guo, X. Qi, C. J. Zhao, H. Zhang, S. C. Wen, D. Y. Tang, and D. Y. Fan, "Broadband nonlinear optical response in multi-layer black phosphorus: an emerging infrared and mid-infrared optical material," Opt. Express **23**(9), 11183–11194 (2015).
5. Y. Wang, G. Huang, H. Mu, S. Lin, J. Chen, S. Xiao, Q. Bao, and J. He, "Ultrafast recovery time and broadband saturable absorption properties of black phosphorus suspension," Appl. Phys. Lett. **107**(9), 091905 (2015).
6. X. Zheng, R. Chen, G. Shi, J. Zhang, Z. Xu, X. Cheng, and T. Jiang, "Characterization of nonlinear properties of black phosphorus nanoplatelets with femtosecond pulsed Z-scan measurements," Opt. Lett. **40**(15), 3480–3483 (2015).
7. D. Hanlon, C. Backes, E. Doherty, C. S. Cucinotta, N. C. Berner, C. Boland, K. Lee, A. Harvey, P. Lynch, Z. Gholamvand, S. Zhang, K. Wang, G. Moynihan, A. Pokle, Q. M. Ramasse, N. McEvoy, W. J. Blau, J. Wang, G. Abellan, F. Hauke, A. Hirsch, S. Sanvito, D. D. O'Regan, G. S. Duesberg, V. Nicolosi, and J. N. Coleman, "Liquid exfoliation of solvent-stabilized few-layer black phosphorus for applications beyond electronics," Nat. Commun. **6**, 8563 (2015).
8. J. Sotor, G. Sobon, M. Kowalczyk, W. Macherzynski, P. Paletko, and K. M. Abramski, "Ultrafast thulium-doped fiber laser mode locked with black phosphorus," Opt. Lett. **40**(16), 3885–3888 (2015).

#263746 http://dx.doi.org/10.1364/OME.6.003159
Journal © 2016 Received 22 Apr 2016; revised 3 Sep 2016; accepted 14 Sep 2016; published 19 Sep 2016

Optical Materials EXPRESS

9. Z. Qin, G. Xie, C. Zhao, S. Wen, P. Yuan, and L. Qian, "Mid-infrared mode-locked pulse generation with multilayer black phosphorus as saturable absorber," Opt. Lett. **41**(1), 56–59 (2016).
10. H. Mu, S. Lin, Z. Wang, S. Xiao, P. Li, Y. Chen, H. Zhang, H. Bao, S. P. Lau, C. Pan, D. Fan, and Q. Bao, "Black phosphorus-polymer composites for pulsed lasers," Adv. Opt. Mater. **3**(10), 1447–1453 (2015).
11. K. Park, J. Lee, Y. T. Lee, W. Choi, J. H. Lee, and Y. Song, "Black phosphorus saturable absorber for ultrafast mode-locked pulse laser via evanescent field interaction," Ann. Phys. (Berlin) **527**(11–12), 770–776 (2015).
12. H. Yu, X. Zheng, K. Yin, X. Cheng, and T. Jiang, "Thulium/holmium-doped fiber laser passively mode locked by black phosphorus nanoplatelets-based saturable absorber," Appl. Opt. **54**(34), 10290–10294 (2015).
13. J. Sotor, G. Sobon, W. Macherzynski, P. Paletko, and K. M. Abramski, "Black phosphorus saturable absorber for ultrashort pulse generation," Appl. Phys. Lett. **107**(5), 051108 (2015).
14. Y. Chen, G. Jiang, S. Chen, Z. Guo, X. Yu, C. Zhao, H. Zhang, Q. Bao, S. Wen, D. Tang, and D. Fan, "Mechanically exfoliated black phosphorus as a new saturable absorber for both Q-switching and Mode-locking laser operation," Opt. Express **23**(10), 12823–12833 (2015).
15. Z. C. Luo, M. Liu, Z. N. Guo, X. F. Jiang, A. P. Luo, C. J. Zhao, X. F. Yu, W. C. Xu, and H. Zhang, "Microfiber-based few-layer black phosphorus saturable absorber for ultra-fast fiber laser," Opt. Express **23**(15), 20030–20039 (2015).
16. J. Ma, S. Lu, Z. Guo, X. Xu, H. Zhang, D. Tang, and D. Fan, "Few-layer black phosphorus based saturable absorber mirror for pulsed solid-state lasers," Opt. Express **23**(17), 22643–22648 (2015).
17. Z. Qin, G. Xie, H. Zhang, C. Zhao, P. Yuan, S. Wen, and L. Qian, "Black phosphorus as saturable absorber for the Q-switched Er:ZBLAN fiber laser at 2.8 μm," Opt. Express **23**(19), 24713–24718 (2015).
18. D. Li, H. Jussila, L. Karvonen, G. Ye, H. Lipsanen, X. Chen, and Z. Sun, "Polarization and thickness dependent absorption properties of black phosphorus: new saturable absorber for ultrafast pulse generation," Sci. Rep. **5**, 15899 (2015).
19. Z. Wang, R. Zhao, J. He, B. Zhang, J. Ning, Y. Wang, X. Su, J. Hou, F. Lou, K. Yang, Y. Fan, J. Bian, and J. Nie, "Multi-layered black phosphorus as saturable absorber for pulsed Cr:ZnSe laser at 2.4 μm," Opt. Express **24**(2), 1598–1603 (2016).
20. V. Tran, R. Soklaski, Y. Liang, and L. Yang, "Layer-controlled band gap and anisotropic excitons in few-layer black phosphorus," Phys. Rev. B **89**(23), 235319 (2014).
21. A. Favron, E. Gaufrès, F. Fossard, A. L. Phaneuf-L'Heureux, N. Y.-W. Tang, P. L. Lévesque, A. Loiseau, R. Leonelli, S. Francoeur, and R. Martel, "Photooxidation and quantum confinement effects in exfoliated black phosphorus," Nat. Mater. **14**(8), 826–832 (2015).
22. Z. Guo, H. Zhang, S. Lu, Z. Wang, S. Tang, J. Shao, Z. Sun, H. Xie, H. Wang, X.-F. Yu, and P. K. Chu, "From black phosphorus to phosphorene: basic solvent exfoliation, evolution of Raman scattering, and applications to ultrafast photonics," Adv. Funct. Mater. **25**(45), 6996–7002 (2015).
23. M. Sheik-Bahae, A. A. Said, T. Wei, D. J. Hagan, and E. W. Vanstryland, "Sensitive measurement of optical nonlinearities using a single beam," IEEE J. Quantum Electron. **26**(4), 760–769 (1990).
24. K. Wang, J. Wang, J. Fan, M. Lotya, A. O'Neill, D. Fox, Y. Feng, X. Zhang, B. Jiang, Q. Zhao, H. Zhang, J. N. Coleman, L. Zhang, and W. J. Blau, "Ultrafast saturable absorption of two-dimensional MoS_2 nanosheets," ACS Nano **7**(10), 9260–9267 (2013).
25. S. Zhang, N. Dong, N. McEvoy, M. O'Brien, S. Winters, N. C. Berner, C. Yim, Y. Li, X. Zhang, Z. Chen, L. Zhang, G. S. Duesberg, and J. Wang, "Direct observation of degenerate two-photon absorption and its saturation in WS_2 and MoS_2 monolayer and few-layer films," ACS Nano **9**(7), 7142–7150 (2015).
26. K. Wang, Y. Feng, C. Chang, J. Zhan, C. Wang, Q. Zhao, J. N. Coleman, L. Zhang, W. J. Blau, and J. Wang, "Broadband ultrafast nonlinear absorption and nonlinear refraction of layered molybdenum dichalcogenide semiconductors," Nanoscale **6**(18), 10530–10535 (2014).
27. Y. Feng, N. Dong, G. Wang, Y. Li, S. Zhang, K. Wang, L. Zhang, W. J. Blau, and J. Wang, "Saturable absorption behavior of free-standing graphene polymer composite films over broad wavelength and time ranges," Opt. Express **23**(1), 559–569 (2015).
28. S. Kumar, M. Anija, N. Kamaraju, K. S. Vasu, K. S. Subrahmanyam, A. K. Sood, and C. N. R. Rao, "Femtosecond carrier dynamics and saturable absorption in graphene suspensions," Appl. Phys. Lett. **95**(19), 191911 (2009).
29. N. Mao, J. Tang, L. Xie, J. Wu, B. Han, J. Lin, S. Deng, W. Ji, H. Xu, K. Liu, L. Tong, and J. Zhang, "Optical anisotropy of black phosphorus in the visible regime," J. Am. Chem. Soc. **138**(1), 300–305 (2016).
30. Y. Xu, Z. Wang, Z. Guo, H. Huang, Q. Xiao, H. Zhang, and X.-F. Xu, "Solvothermal synthesis and ultrafast photonics of black phosphorus quantum dots," Adv. Opt. Mater. **4**(8), 1223–1229 (2016).

1. Introduction

The black phosphorus (BP) has gained much attention recently due to its unique band structure, superior electronic and optical properties comparing with its two-dimensional counterparts like MoS_2 and graphene [1–3]. BP is a broad band saturable absorber covering the whole UV-Mid infrared range. S.-B. Lu et al. demonstrated that BP showed saturable absorption (SA) ranging from the visible (400 nm) towards mid-IR (at least 1930 nm) [4,5]. X. Zheng et al. has also observed the SA and two-photon absorption (TPA) of BP

Optical Materials EXPRESS

nanoplatelets at 800 nm and they have measured the nonlinear refractive index with closed-aperture configuration [6]. When compared with the typical broad band saturable absorber graphene, BP also exhibits better performance with lower saturable intensity [7]. Thereafter, BP has been utilized as an ultrafast saturable absorber device in the mode-locking of a thulium-doped fiber laser operating in the 2 μm wavelength range [8]. Pulses centered at 1910 nm with pulse width of 739 fs were generated. BP mode-locked laser at 2.8 μm with pulse duration of 42 ps has also been demonstrated [9]. Although BP has been widely used as an ascendant saturable absorber in Q-switching and mode-locking [10–19], the size and layer number dependence of SA for BP remains unexplored. In this paper, we have prepared three types of BP dispersions with different sizes utilizing the liquid phase exfoliation method. The SA property was investigated by Z-scan technique and the parameters were obtained by fitting the data with analytical solution of the propagation equation. The SA coefficients, imaginary part of the third order optical susceptibility of the different dispersions are compared at two specific wavelengths, one above the bandgap of the BP monolayer at 515 nm and another between the bandgaps of the monolayer and bulk at 1030 nm. The figure of merit was employed to assess the SA performance. In the end, our BP nanosheets have been successfully used as saturable absorber in the mode-locking application.

2. Experimental

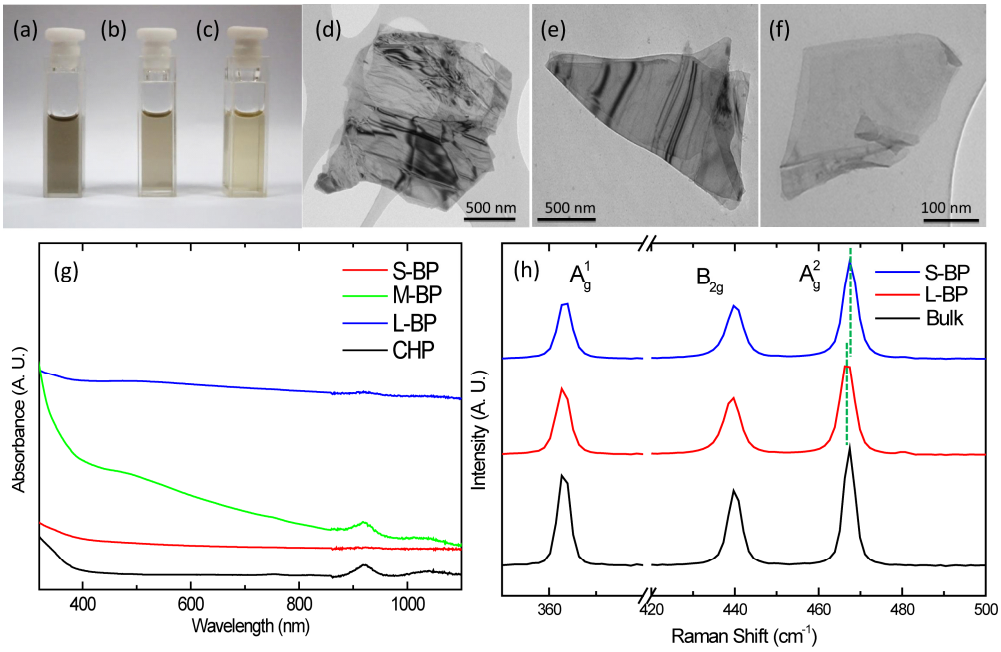

Fig. 1. The images of large (a), medium (b) and small (c) BP/CHP dispersions in quartz cuvettes. (d-f) are TEM images of large, medium and small BP nanosheets (L-BP, M-BP and S-BP). (g, h) are linear absorption spectra of BP nanosheets, pure CHP and Raman spectra of S-BP, L-BP and bulk powder.

Black phosphorus crystal was purchased from Smart elements and used as received. It was crushed and then sonicated in cyclohexyl pyrrolidone (CHP). The resulting dispersion was then subjected to a series of centrifugation steps to isolate nanosheets with varying sizes. Firstly the dispersion was centrifuged at 1000 rpm for 180 mins to remove any unstable nanomaterial. The supernatant was decanted and subjected to one more centrifugation step at medium speed (5000 rpm, 2,660 *g*, 2 h) and collected supernatant containing "small nanosheets", S-BP, middle part containing "medium nanosheets", M-BP and redispersed the sediment containing "larger nanosheets", L-BP. This bears the advantage that we start from

Optical Materials EXPRESS

the well characterized dispersion that already only contains nanosheets which are stable (i.e. those are not sedimenting), as the centrifugation time for the first centrifugation step was optimized. Figures 1(a)-1(c) shos the images of BP/CHP dispersions containing large, medium and small BP nanosheets in quartz cuvettes.

Bright-field TEM imaging was performed using a JEOL 2100 (at 200 kV). Figures 1(d)-1(f) are the TEM images of L-BP, M-BP and S-BP, respectively. The liquid phase exfoliation procedure gives dispersions with mean nanosheet lengths of about 130 nm in the case of S-BP, 1.50 μm for the M-BP and 2.26 μm in the case of L-BP. The details of TEM characterization and atomic force microscopy (AFM) statistics were described in our previous paper and its supplementary information [7]. The nanosheet size is in agreement with that from AFM statistical analysis. The average layer number of S-BP, M-BP and L-BP can be roughly estimated as <3~5>, <12~14>, and <15~17>, respectively, using the empirical formula: $N \propto \sqrt{A}$, where A is the flake area [7]. In Figs. 1(a)-1(c), it is visible to the naked eyes that the linear transmittance increases when the size of nanosheets decreases in 10 × 10 mm cuvettes, while it is not obvious in 10 × 1 mm ones. This is understandable as large size BP nanosheets with larger layer number have smaller bandgap, which can be estimated using the formula $E_g \approx (1.7/n^{0.73} + 0.3)$ eV [20], resulting greater linear absorbance in the visible range.

The optical absorbance spectra of S-BP, M-BP and L-BP were measured using a Perkin Elmer Lambda 750 spectrometer in 10 mm × 1 mm quartz cuvettes. Pure CHP was also measured for comparison. In Fig. 1(g), it can be seen that the absorbance of S-BP, M-BP and L-BP decreases gradually from 300 nm to 1100 nm. Obviously, there is no absorption peak for BP during this range. The absorption peak of CHP around 920 nm is negligible for S-BP and L-BP dispersions. All S-BP, M-BP and L-BP dispersions have smooth absorption in the UV-NIR wavelength range, indicating BP is a broadband absorber. Raman spectra of S-BP, L-BP and bulk powder were taken using a Horiba Jobin Yvon LabRam HR800 with a 633 nm excitation laser. Three characteristic peaks correspond to one out-of-plane vibration mode A_g^1 and two in-plane vibration modes B_{2g}, A_g^2, as shown in Fig. 1(h). The layer number can be estimated from the Raman peak position and full-width at half-maximum (FWHM) [21, 22]. We found that the Raman peak position dependence on the layer number was in agreement with [21]. The in-plane vibrational mode A_g^2 of S-BP sample located at 467.6 cm^{-1} and the thickness can be estimated as ~2.2 nm. Hence, the layer number can be determined to be about 4~5, in the range of the average layer number <3~5> for the S-BP nanosheet dispersion. This is in good agreement with the estimation using the empirical formula. The A_g^2 position of L-BP and bulk located at ~466.5 cm^{-1} and 466.3 cm^{-1}, repectively. The layer number of L-BP cannot be precisely estimated from the Raman peak position and we used the empirical formula of $N \propto \sqrt{A}$ and found it in the range of <15-17>.

We utilized an open-aperture Z-scan system to study the size (layer) dependence of the SA properties of BP. The laser beam traverses through a lens with focal length of 150 mm. The sample is translated through the beam waist using a motorized translation stage [23, 24]. All experiments were performed with a mode-locked fiber laser, which was operated at 1030 nm and its second harmonic, 515 nm, with a pulse width of 340 fs and a repetition rate of 1 kHz. The beam waist radius was ~32 μm at 1030 nm and ~16 μm at 515 nm. All samples were tested in quartz cuvettes with 1 mm pathlength. The precision of this system was confirmed by our previous measurements of graphene/PVA films, MoS_2 nanoflake dispersions and WS_2 films [24–27]. For example, the figure of merit (FOM) = $|Im\chi^{(3)}/\alpha_0|$ of graphene/PVA films was about (9.3 ± 4.4) × 10^{-15} esu cm, in a good agreement with the reported result of ~5.0 × 10^{-15} esu cm [28].

Optical Materials EXPRESS

3. Results and discussion

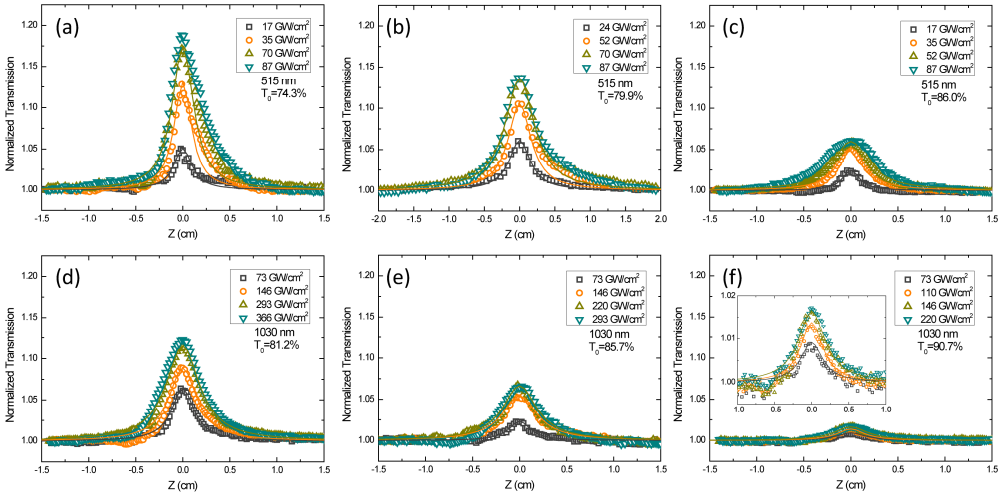

Fig. 2. The saturable absorption of L-BP (a), M-BP (b), S-BP (c) at 515 nm and 1030 nm (d-f).

BP is a direct bandgap semiconductor and its bandgap decreases from about 2 eV (~620 nm) for monolayer to about 0.3 eV (~4133 nm) for bulk [1, 20]. Thus, to investigate the size dependence of SA of BP, we selected two wavelengths 515 nm and 1030 nm for laser excitation: one lies beyond the bandgap of monolayer and the other one lies between monolayer and bulk. The linear transmittance of L-BP, M-BP and S-BP dispersions was measured to be 74.3%, 79.9%, 86.0% at 515 nm and 81.2%, 85.7%, 90.7% at 1030 nm, respectively. Figures 2(a)-2(c) show the Z-scan results of L-BP, M-BP and S-BP dispersions at 515 nm. In Fig. 2(a), the amplitude of the SA (corresponding to the normalized transmission) increases to a maximum when the intensity of the incident laser beam increases gradually to 70 GW/cm^2, meaning that the extent of SA has reached the limit. Within the energy range $\Delta E = E-E_g$ (E is the excitation energy, E_g is the bandgap), all electron states near the bottom of the conduction band are filled, the so-called state-filling effect. When the incident intensity increases continuously to 87 GW/cm^2, the amplitude of the SA almost keeps the same. If the excitation intensity keeps growing, other optical nonlinear effects like excited-state absorption, TPA may become apparent. The reasonable analysis of SA for a material should be based on the results below maximum excitation intensity. When comparing Figs. 2(a)-2(c), it can be seen that when the size of the nanosheets decreases, the maximum amplitude $(T-T_0)/T_0$ decreases from ~19% to ~6.3%. It is easy to understand because the maximum amplitude positively correlates to ΔE. When the mean size of the nanosheets decreases, the average layer number becomes smaller, resulting larger energy bandgap E_g and thus smaller ΔE, smaller maximum amplitude. Figure 2(d-f) shows the Z-scan results of L-BP, M-BP and S-BP dispersions at 1030 nm. Similar to the case at 515 nm, the maximum amplitude also decreases from ~13% to ~2.1% when the size of the nanosheets decreases. When comparing Fig. 2(a) and Fig. 2(d), it can be seen that the maximum amplitude decreases from ~19% to ~13%. It is due to smaller excitation energy E (1.204 eV<2.408 eV) resulting in a smaller ΔE. The excitation intensities are much larger at 1030 nm than those at 515 nm, which might be due to the smaller dipole oscillator strength at that wavelength. This can also be inferred from the smaller linear absorption of BP at 1030 nm than that at 515 nm, as shown in Fig. 1(g).

Optical Materials EXPRESS

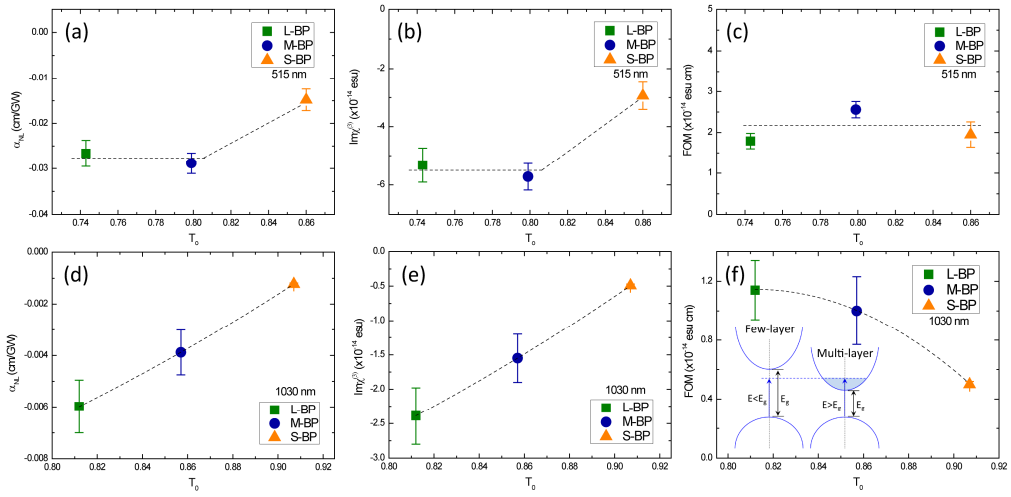

Fig. 3. The saturable absorption coefficient α_{NL} (a), imaginary part of $\chi^{(3)}$ (b), figure of merit FOM (c) of L-BP, M-BP and S-BP at 515 nm and 1030 nm (d-f).

We analyzed the Z-scan results with the excitation intensity below the maximum one as explained above. The nonlinear beam propagation model was widely used in thin films, liquids, dispersions, etc. [23].

$$\frac{dI(z')}{dz'} = -\alpha_0 I(z') - \alpha_{NL} I^2(z'), \tag{1}$$

where $I(z')$ is the laser beam irradiance within the sample, z' is the propagation distance in the sample, α_0 is the linear absorption coefficient and α_{NL} is the nonlinear absorption coefficient, which means the SA here. The normalized power transmission can be obtained by analytically solving Eq. (1).

$$T(z) = \frac{\ln[1+q_0(z)]}{q_0(z)}, \tag{2}$$

where $q_0(z) = \alpha_{NL} I_0 L_{eff} / (1+z^2/z_0^2)$, $L_{eff} = (1-e^{-\alpha_0 L})/\alpha_0$ is the sample's effective thickness, I_0 is the on-axis irradiance at the focus, z_0 is the beam's diffraction length.

The Z-scan curves were fitted by utilizing Eq. (2). The SA coefficients α_{NL} of L-BP, M-BP and S-BP at 515 nm were obtained, as shown in Fig. 3(a). The horizontal axis is the linear transmittance. The data points at 74.3%, 79.9% and 86.0% correspond to L-BP, M-BP and S-BP with sizes of <2.26 μm>, <1.50 μm> and <130 nm>. It can be seen that α_{NL} is almost the same for L-BP, M-BP at 515 nm, while for S-BP the absolute value decreases. The imaginary part of the third-order nonlinear optical susceptibility $\mathrm{Im}\,\chi^{(3)}$ can be calculated from α_{NL}.

$$\mathrm{Im}\,\chi^{(3)} = \frac{10^{-7} c\lambda n^2}{96\pi^2}\alpha_{NL}, \tag{3}$$

where c is the velocity of light, λ is the wavelength of the incident light and n is the linear refractive index, about 3.5 for BP [29]. The $\mathrm{Im}\,\chi^{(3)}$ of L-BP, M-BP and S-BP are shown in Fig. 3(b), the same variation trend with α_{NL}. When assessing the performance of a saturable

Optical Materials EXPRESS

absorber, it is better to eliminate the discrepancy caused by the linear absorption α_0. Therefore, the figure of merit (FOM) was defined as: FOM = $|\mathrm{Im}\,\chi^{(3)}/\alpha_0|$. Figure 3(c) shows the FOM of L-BP, M-BP and S-BP and they are at the same level at 515 nm. The α_{NL} and $\mathrm{Im}\,\chi^{(3)}$ at 1030 nm decrease almost linearly with the linear transmittance when the size of nanosheets becomes smaller, as shown in Fig. 3(d-e). When comparing Fig. 3(c) with Fig. 3(f), we can find that the FOM at 515 nm hardly depends on the size (layer number) of the BP nanosheets, whereas that at 1030 nm decreases gradually when the size becomes smaller. It can be well explained from the band structure of few-layer and multi-layer BP in the inset of Fig. 3(f). As the bandgap of BP decreases from ~2.0 eV for monolayer to ~0.3 eV for bulk, all BP nanosheets in L-BP, M-BP and S-BP will exhibit SA with 515 nm (2.408 eV>2.0 eV) excitation, leading to almost the same FOM. At 1030 nm (1.204 eV) excitation, the SA would not occur for mono- and bilayer (~1.325 eV) BP nanosheets. Only multi-layer BP nanosheets whose bandgap is smaller than 1.204 eV contribute to the SA. Thus the FOM decreases for S-BP dispersion. The SA parameters of L-BP, M-BP and S-BP dispersions with different linear transmittance are summarized in Table 1. The SA coefficient α_{NL} at 515 nm is comparable to the reported result at 400 nm: $(-1.62 \pm 0.28) \times 10^{-2}$ cm/GW [4]. It can be seen that although the FOM decreases slightly with the size at 1030 nm, it is still in the same order of magnitude with that at 515 nm, indicating that BP is a good broadband saturable absorber. Xu et al. prepared the BP quantum dots by solvothermal synthesis and found that the SA property is much better than that of BP nanosheets [30]. The average lateral size of the BP QDs is only about 2.1 ± 0.9 nm, in which the quantum confinement effect might be dominant. In our case, although the average lateral size of the S-BP nanosheets is about 130 nm, the size is still far from that of quantum dots. The band structure was to be considered in terms of few-layer BP without any quantum confinement effect. The saturation intensity was obtained using the saturation model in our previous work [7] and it was about 300 GW/cm^2 at 1030 nm, much larger than that of BP QDs (only 3.3 GW/cm^2 at 800 nm) but in the same order of magnitude with Xu et al. (535.3 GW/cm^2 at 800 nm) and Lu's results (647.7 ± 60 at 800 nm) about BP nanosheets [4, 30].

Table 1. Saturable absorption parameters for L-BP, M-BP and S-BP at 515 nm and 1030 nm

Wavelength (nm)	T_0 (%)	α_0 (cm^{-1})	Mean flake size	Mean layer number (L)	α_{NL} ($\times 10^{-2}$ cm/GW)	$\mathrm{Im}\chi^{(3)}$ ($\times 10^{-14}$ esu)	FOM ($\times 10^{-14}$ esu cm)
515	74.3	2.97	<2.26 μm>	<15~17>	−2.66 ± 0.29	−5.32 ± 0.58	1.79 ± 0.19
	79.9	2.24	<1.50 μm>	<12~14>	−2.88 ± 0.22	−5.72 ± 0.45	2.56 ± 0.20
	86.0	1.51	<130 nm>	<3~5>	−1.48 ± 0.24	−2.94 ± 0.47	1.95 ± 0.31
1030	81.2	2.08	<2.26 μm>	<15~17>	−0.60 ± 0.10	−2.39 ± 0.41	1.14 ± 0.20
	85.7	1.54	<1.50 μm>	<12~14>	−0.39 ± 0.09	−1.55 ± 0.35	1.00 ± 0.23
	90.7	0.98	<130 nm>	<3~5>	−0.123 ± 0.004	−0.49 ± 0.02	0.50 ± 0.02

Optical Materials EXPRESS

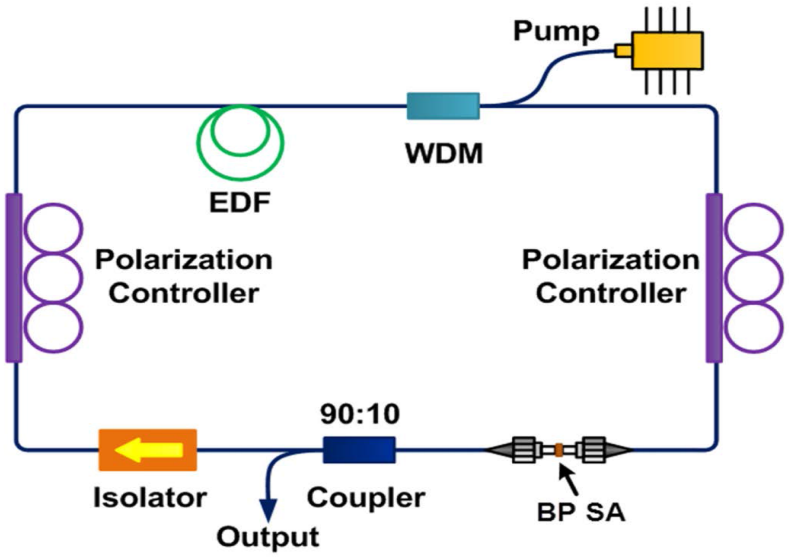

Fig. 4. Q-switched laser incorporated with BP nanosheet dispersions.

The Q-switching operation of BP saturable absorber has been demonstrated. The laser design was shown in Fig. 4. 976 nm pump was injected into the Erbium-doped fiber (EDF) via a wavelength division multiplexer (WDM) to provide gain in the laser cavity. Two polarization controllers were used to adjust the birefringence for a stable Q-switching operation. L-BP was prepared in a transparent cell and it was embedded between two fiber connectors so that the light field can directly interact with the sample. The light was extracted by a 90:10 coupler as output and the uni-directional operation was guaranteed by an isolator.

A standard two-arm transmission measurement is conducted to investigate the saturable absorption near 1560 nm. The mode-locked laser source has a repetition rate of 37 MHz, a center wavelength of 1560 nm and a pulse width of ~500 fs. The measured saturable absorption is shown in Fig. 5. It can be found that the saturation intensity is ~50 MW/cm^2 and the modulation depth is 3.45%.

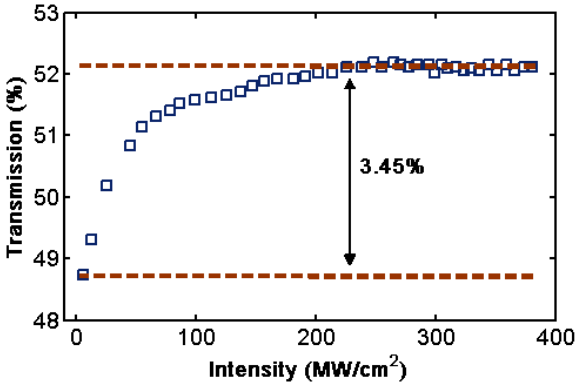

Fig. 5. Saturable absorption of black phosphorus nanosheets (L-BP).

The mode-locking operation was obtained and characterized. The output properties of the laser are summarized in Fig. 6. The optical spectrum shown in Fig. 6(a) has a center wavelength of 1555 nm and a 3-dB bandwidth of 4.6 nm. The autocorrelation trace of the output pulse is shown in Fig. 6(b). The time width is 1.06 ps, corresponding to a pulse width of 687 fs assuming a sech^2 profile. The time-bandwidth product is 0.392. It is larger than the TBP of a transform limited pulse meaning the pulse is chirped. This is due to the fiber pigtail

Optical Materials EXPRESS

outside the fiber. The oscilloscope trace is shown in Fig. 6(c). The repetition frequency is 37.8 MHz. Very flat pulse amplitude can be found which indicates the stable mode locking operation. The relation between the pump power and laser output power is shown in Fig. 6(d). The mode locking is obtained when the pump power exceeds 240 mW.

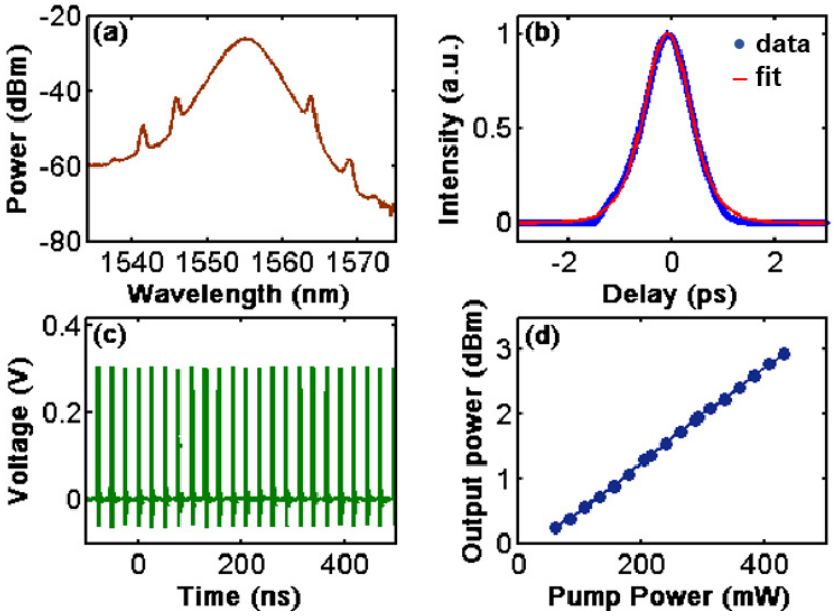

Fig. 6. (a) Optical spectrum, (b) autocorrelation trace, (c) oscilloscope trace and output power vs. pump power of the mode-locked laser based on black phosphorus.

The electrical spectrum of the laser is also investigated to further confirm the stability of the mode locking operation, shown in Fig. 7. Figure 7(a) shows the electrical spectrum over a span of 500 MHz with a resolution bandwidth (RBW) of 100 kHz. A finer spectrum is shown in Fig. 7(b) with a span of ~15 MHz and a RBW of 100Hz. An extinction ratio of 80 dB is observed, indicating the highly stable mode locking operation.

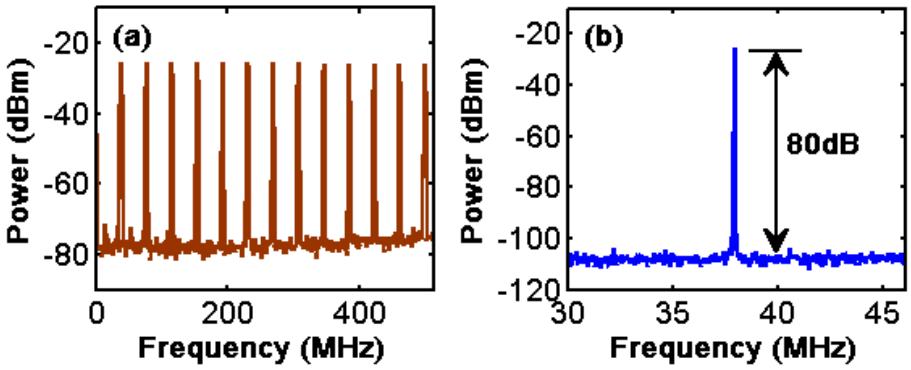

Fig. 7. (a) RF spectrum with a span of 500 MHz and a RBW of 100 kHz; (b) RF spectrum with a span of 15 MHz and a RBW of 100 Hz.

4. Conclusion

In summary, we have investigated the size dependence of SA properties for BP at 515 nm and 1030 nm. The amplitude of SA reached a maximum when the incident intensity increases. It decreases when either the size of the BP nanosheets or the excitation energy becomes smaller.

Optical Materials EXPRESS

This can be well explained with the formula $\Delta E = E\text{-}E_g$. At 515 nm, α_{NL} and $\mathrm{Im}\,\chi^{(3)}$ are almost the same for L-BP, M-BP, and while for S-BP they decrease. The α_{NL} and $\mathrm{Im}\,\chi^{(3)}$ at 1030 nm decrease almost linearly with the linear transmittance when the size of nanosheets becomes smaller. The FOM at 515 nm hardly depends on the size (layer number) of the BP nanosheets, about $(2.1 \pm 0.3) \times 10^{-14}$ esu cm, whereas that at 1030 nm decreases from $(1.14 \pm 0.20) \times 10^{-14}$ to $(0.50 \pm 0.02) \times 10^{-14}$ esu cm when the size of nanosheets in dispersion becomes smaller. The mode-locking operation was obtained and characterized. The center wavelength is 1555 nm with a 3-dB bandwidth of 4.6 nm. It implies the potential application of BP in nanophotonic device, such as mode-lockers, Q-switchers, optical switches, etc.

Funding

National Natural Science Foundation of China (NSFC) (No. 61308034, No. 61522510, No. 51302285, No. 61505105, No. 61675217); External Cooperation Program of BIC, CAS (No. 181231KYSB20130007); Shanghai Yangfan Program (No. 14YF1401600); State Key Lab Project of Shanghai Jiao Tong University (No. GKZD030033); European Research Council (SEMANTICS); SFI (11/PI/1087); SFI funded centre AMBER (SFI/12/RC/2278); EU FP7 Graphene Flagship (604391); and Key Research Program of Frontier Science, CAS (No. QYZDB-SSW-JSC041).